催化学报
2012 Chinese Journal of Catalysis Vol. 33 No. 2

Article ID: 0253-9837(2012)02-0247-07 **DOI**: 10.1016/S1872-2067(10)60276-8 **Article:** 247–253

H_2 Production with Low CO Selectivity from Photocatalytic Reforming of Glucose on Ni/TiO_2-SiO_2

R. M. MOHAMED[1,2,3,*], Elham S. AAZAM[1]

[1]*Chemistry Department, Faculty of Science, King Abdulaziz University, Jeddah 21589, King Saudi Arabia*

[2]*Nanostructured Materials Division, Advanced Materials Department, Central Metallurgical R&D Institute, Helwan 11421, Cairo, Egypt*

[3]*Center of Excellence in Environmental Studies, King Abdulaziz University, P.O. Box 80216, Jeddah 21589, Saudi Arabia*

Abstract: Nano-sized Ni particles on TiO_2-SiO_2 were synthesized by the two methods of photo-assisted deposition (PAD) and impregnation. H_2, which is a promising energy carrier, with a low CO concentration was produced by the photocatalytic reforming of glucose (a model biomass) on the Ni/TiO_2-SiO_2 catalyst. The supported Ni enhanced the rate of H_2 production while it suppressed CO selectivity. The catalysts were characterized by X-ray diffraction, X-ray absorption fine structure, transmission electron microscope, and nitrogen adsorption analysis. Both H_2 production and CO selectivity were strongly dependent on the preparation method, and PAD-Ni/TiO_2-SiO_2 was the better catalyst for H_2 production with the lowest CO concentration.

Key words: titanium dioxide; silicon dioxide; nickel doping; hydrogen production

CLC number: O643 **Document code:** A

Received 14 June 2011. Accepted 3 September 2011.

**Corresponding author. Tel: +966-26952031; Fax: +966-26400376; E-mail: redama123@yahoo.com*

English edition available online at Elsevier ScienceDirect (http://www.sciencedirect.com/science/journal/18722067).

Hydrogen has been identified as an ideal energy carrier for sustainable energy development [1–4]. Hydrogen can be used in a fuel cell to generate electricity with high efficiency. It is extremely clean because the only byproduct is water. In order to support a sustainable hydrogen economy, it is crucial to produce hydrogen cleanly and renewably. In the past two decades, most investigations have focused on photocatalytic hydrogen production and the electronic structures of semiconductor catalysts containing d^0 metal ions [5–11] such as Ti^{4+}, Zr^{4+}, Nb^{5+}, and Ta^{5+}. However, the photocatalytic efficiency of most semiconductor photocatalysts is too low for them to be applied in industry. This is mainly caused by photogenerated electron-hole recombination in the bulk or at the surface of the photoexcited catalyst particles. Therefore, considerable efforts have been devoted to improving the efficiency of H_2 production by modifying the nanostructures of the metal oxides [12–15], as well as developing new photocatalysts [16–20]. Furthermore, semiconductor metal oxides are also often the photocatalysts for the light induced photo-oxidation of water.

Titanium dioxide is a very well studied UV-responsive photocatalyst because of its energy band gap in the range of 3.0–3.2 eV [21]. Anatase and rutile are the two polymorphic forms of TiO_2 that are relevant to photocatalytic applications [22]. Anatase is generally more photocatalytically active than rutile [23–27]. Anatase is a well-known and studied photocatalyst, [28] but its polymorphic transformation to rutile often limits its usefulness. A high specific surface area [29] and crystallinity [30] enhance photocatalytic activity.

The supporting of metal oxides on oxide carriers can result in an enhancement of the activity for oxidation. For example, when vanadia was supported on TiO_2-anatase, the resulting complex was more active for both the selective oxidation of various hydrocarbons [31,32] and for the selective catalytic reduction of NO_x by ammonia (SCR reaction) [33].

In the literature, several metal oxides, such as Al_2O_3, ZrO_2, and SiO_2 [34–36], have been added to titania to improve its UV photocatalytic activity. The addition of silica to TiO_2 resulted in properties such as the ability to maintain a charge and is particularly attractive because silica is a low-cost, non-toxic, and readily available material. Moreover, titanium dioxide is compatible with the processing of silicate body mixes, and the possibility of obtaining photocatalytically active building materials could be another way to fight rising environmental pollution.

The full environmental benefit of moving towards a hydrogen society will be realized only when H_2 is produced from renewable resources, such as biomass and water. The technologies for generating hydrogen from biomass, such as gasification and steam-reforming of bio-oils, suffer from huge heat use, and complex processing requirements [37,38]. Dumesic et al. [39,40] recently reported that hy-

drogen can be generated by the catalytic reforming of biomass-derived hydrocarbons in aqueous solution at temperatures near 500 K in a single reactor, aqueous phase reforming process. Some byproducts, such as gaseous alkanes, were present in the H_2 and the reaction took place under high pressure. The photocatalytic reforming of biomass, which preserves solar energy as chemical energy, is a promising way to produce hydrogen. Kawai et al. [41,42] have demonstrated photocatalytic H_2 production from decomposition of protein, algae, dead insects, excrement, and sugars on TiO_2 catalysts, where only CO_2 was the byproduct.

Glucose, which is the major energy resource in plants and animals, was taken as a model for biomass in this work. CO selectivity, besides H_2 production, is of concern because CO easily poisons the noble metal based catalysts in fuel cells at even very low concentrations. In this work, two preparation methods were used to synthesize Ni/TiO_2-SiO_2, and for comparison, the photocatalytic and textural properties of the Ni/TiO_2-SiO_2 catalysts were evaluated. The influences of various factors on the photocatalytic activity were correlated.

1 Experimental

1.1 Synthesis of TiO_2-SiO_2

The TiO_2-SiO_2 complex was synthesized using titanium tetrabutoxide (TBOT, ≥ 98%) and tetraethyl orthosilicate (TEOS, ≥ 98%). TBOT was mixed in a solution of acetylacetone and anhydrous ethyl alcohol, while TEOS was dissolved in a solution of water, ammonia, and ethyl alcohol with vigorous stirring. Next, the resulting sols were added dropwise into a solution of anhydrous ethyl alcohol while stirring to avoid metal hydroxide precipitation. The hydrolyzed alkoxides were aged at room temperature for 72 h. The samples obtained were dried under vacuum at room temperature, followed by calcination at 550 °C for 5 h under a air atmosphere.

1.2 Photocatalyst synthesis

Ni was loaded onto TiO_2-SiO_2 (5 wt% Ni content) using two different methods: photo-assisted deposition (PAD) and impregnation. For the PAD method, the deposition of Ni on TiO_2-SiO_2 was conducted in an aqueous solution of nickel nitrate with UV-light irradiation. For impregnation method, the deposition of Ni was conducted in the absence of light in an aqueous solution of nickel nitrate. The impregnation and PAD precursors with 5 wt% Ni content were oven-dried at 378 K followed by H_2 reduction (20 ml/min) at 473 K for 2 h. These samples are referred to according to their preparation routes: PAD-Ni-TiO_2-SiO_2 or img-Ni-TiO_2-SiO_2.

1.3 Photocatalyst characterization

For the morphology observation of the prepared samples, transmission electron microscopy (TEM) using a Hitachi H-9500 apparatus operated at 300 kV was used. The crystalline phases were identified by X-ray diffraction (XRD) using a Rigaku RINT 2000 diffractometer with Cu K_α radiation, $\lambda = 0.15406$ nm).

The textural properties of the samples were evaluated from the adsorption-desorption isotherms of nitrogen using a Nova2000 series apparatus (Chromatech). The specific surface areas of the materials were calculated using the BET method and the 0.005–0.3000 range of relative pressure (p/p_0). Prior to adsorption, the samples were degassed under vacuum at 270 °C for 5 h.

Diffuse reflectance ultraviolet-visible absorption spectra (DRS UV-Vis) were collected with the aim to detect whether nickel addition had shifted the titania absorption edge. Spectra were acquired in the UV-Vis range (200–800 nm) with $BaSO_4$ as reference and recorded on a Shimadzu UV-2450 spectrophotometer at 295 K. They were converted from reflection to absorbance by the standard Kubelka-Munk method.

The X-ray absorption fine structure (XAFS), X-ray absorption near edge structure (XANES), and extended X-ray absorption fine structure (EXAFS) spectra were measured at the BL-7C facility of the Photon Factory at the National Laboratory for High-Energy Physics, Tsukuba. A Si(111) double crystal was used to monochromatize the X-rays from the 2.5 GeV electron storage ring. The Ni K-edge absorption spectrum was recorded in the fluorescence mode at 298 K. The normalized spectra were obtained by a reported literature procedure [43], and Fourier transforms were performed on κ^3-weighted EXAFS oscillations in the range of 0.3–1 nm^{-1}.

1.4 Photocatalytic activity

The photocatalytic reaction was performed in an inner irradiation reactor connected to a closed gas circulation and evacuation system. Typically, 0.5 g powder of catalyst was dispersed in the reactor containing 800 ml glucose aqueous solution. A 300 W high pressure Hg lamp inside the reactor irradiated the reaction system. To avoid heating of the solution during the reaction, cooling water was circulated through a cylindrical quartz jacket located around the light source to remove the infrared (IR) light illumination from the Hg lamp. Prior to the reaction, the suspension was deaerated by evacuation. The gaseous products were periodically analyzed by an online gas chromatograph (Shanghai GC-920, TDX-01 carbon molecular sieve packed column, Ar carrier gas). The chromatograph was equipped with

a thermal conductivity detector, a flame ionization detector, and a methanizer. H_2 concentration was measured by the thermal conductivity detector. The flame ionization detector was used to analyze CO, which was converted into CH_4 by the methanizer. The detection limit of CO was 5×10^{-6}. The response factors for the gas products were obtained by using appropriate standards.

2 Results and discussion

2.1 Synthesis and characterization

2.1.1 XRD results

The XRD patterns of the samples are shown in Fig. 1. All samples had a single phase that was identified as anatase. This indicated that all the samples from the PAD and "imp" experiments were converted to the anatase phase. No Ni oxide peaks were found in the patterns from the Ni-doped samples. The absence of Ni signals can be attributed to the low Ni doping content (*ca.* 5 wt%). The data indicated that Ni was well dispersed within the TiO_2-SiO_2 phase.

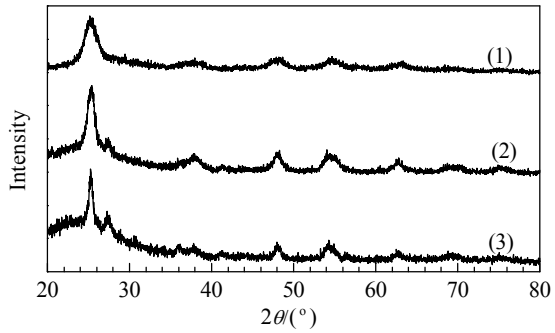

Fig. 1. XRD patterns of the TiO_2-SiO_2 (1), PAD-Ni-TiO_2-SiO_2 (2), and img-Ni-TiO_2-SiO_2 (3).

2.1.2 DRS UV-Vis results

UV-Vis measurements were made to determine the energy band gap. The UV-Vis diffuse reflectance spectra for the samples are shown in Fig. 2. An intense absorption onset in the range of 350–400 nm was found for Ni/TiO_2-SiO_2, while TiO_2-SiO_2 only absorbed UV-light with wavelengths less than 300 nm.

The Kubelka-Munk function, F(R), is considered proportional to the absorption of radiation [44]. On this basis, the band gap of the semiconductor, E_g, can be derived from the spectra by plotting $(F(R)\cdot h\nu)^{1/2}$ against $h\nu$ [45]. The E_g values obtained are summarized in Table 1. These values were influenced by various factors in the synthesis procedure, such as the existence of doping impurities, crystalline network, and average crystal size of the semiconductor. In addition, different methods for calculating E_g from UV-Vis reflectance spectra can give discrepancies. For example, some authors have calculated E_g values by a direct extrapolation from the F(R) spectrum, whereas others have reported the wavelength corresponding to maximum absorption [47]. Consequently, the reported E_g values for rutile and anatase samples vary widely in the literature. For anatase-based materials, threshold wavelength values of 370 [46], 380 [48], 387 [49], 393 [46], and 403 nm [50] corresponding to a band gap range from 3.08 to 3.35 eV have been reported. In the case of rutile-based materials, an absorption wavelength as high as 437.4 nm (E_g = 2.84 eV) has been given [50]. In the present study, the values calculated for TiO_2-SiO_2, PAD-Ni-TiO_2-SiO_2, and img-Ni-TiO_2-SiO_2 were 3.35, 2.85, and 3.05 eV, respectively. Therefore, the order of the band gap energy is PAD-Ni-TiO_2-SiO_2 < img-Ni-TiO_2-SiO_2 < TiO_2-SiO_2. These data clearly indicate that the use of UV-Vis absorption constitutes an important tool for evaluating the changes produced in semiconductor materials by different preparation methods.

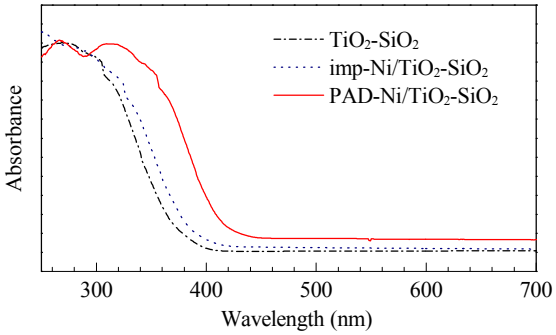

Fig. 2. UV-Vis diffuse reflectance spectra of TiO_2-SiO_2, PAD-Ni/TiO_2-SiO_2, and img-Ni/TiO_2-SiO_2.

Table 1 Calculated band gap energy of TiO_2-SiO_2, PAD-Ni-TiO_2-SiO_2, and img-Ni-TiO_2-SiO_2

Sample	Band gap energy (eV)
TiO_2-SiO_2	3.35
PAD-Ni-TiO_2-SiO_2	2.85
img-Ni-TiO_2-SiO_2	3.05

2.1.3 Specific surface area

The textural properties of the samples were evaluated using N_2 adsorption-desorption isotherms. Specific surface area (S_{BET}), total pore volume (V_p), and average pore diameter (r) data are reported in Table 2. The incorporation of Ti^{4+} ions into SiO_2 had multiple effects on the final textural properties of the samples, which were probably based on the nature of the precursors [51].

The BET surface area measurements revealed that the

Table 2 Textural parameters of TiO_2-SiO_2, img-Ni-TiO_2-SiO_2, and PAD-Ni-TiO_2-SiO_2

Sample	S_{BET} (m^2/g)	S_t (m^2/g)	S_{micro} (cm^2/g)	S_{meso} (cm^2/g)	S_{ext} (cm^2/g)	V_p[6] (cm^3/g)	V_{micro} (cm^3/g)	V_{meso}[8] (cm^3/g)	r[9] (nm)
TiO_2-SiO_2	510	507	400	100	400	0.400	0.093	0. 307	2.95
img-Ni-TiO_2-SiO_2	550	554	440	110	440	0.426	0. 105	0.321	2.94
PAD-Ni-TiO_2-SiO_2	660	655	550	108	555	0.481	0. 102	0.379	2.85

S_{BET}—BET-Surface area; S_t—surface area derived from $V_{l\text{-}t}$ plots; S_{micro}—surface area of micropores; S_{meso}—surface area of mesopores; S_{ext}—external surface area; V_p—total pore volume; V_{micro}—pore volume of micropores; V_{meso}—pore volume of mesopores; r—mean pore radius.

loading of Ni by either of the two methods gave a significant increase in the surface area of img-Ni-TiO_2-SiO_2 and PAD-Ni-TiO_2-SiO_2 compared with TiO_2-SiO_2 (Table 2). The surface area changed from 510 (parent TiO_2-SiO_2) to 550 and 660 m^2/g for img-Ni-TiO_2-SiO_2 and PAD-Ni-TiO_2-SiO_2, respectively. This corresponded to 7.8% (img) and 29% (PAD) increases in the surface area as compared to the parent TiO_2-SiO_2.

The N_2 adsorption isotherms (not shown here) for the parent and the Ni/TiO_2-SiO_2 samples were typical of mesoporous solids (Type IV). However, the addition of Ni ions resulted in an increase in the adsorption capacity. Furthermore, the total pore volumes of the two Ni/TiO_2-SiO_2 complexes were higher than that of TiO_2-SiO_2. The values of S_{BET} and S_t were very similar for all samples, indicating the presence of mesopores. Finally, the values of S_{mic} were high compared to those of S_{mes}, implying that the main surfaces were in the mesopores in agreement with the isotherms. The correlation between the surface textural data and catalytic activity will be discussed in a later section.

2.1.4 EXAFS analysis

The Fourier transforms of the Ni K-edge EXAFS spectra for PAD-Ni-TiO_2-SiO_2, img-Ni-TiO_2-SiO_2, and two references (Ni foil and NiO) are displayed in Fig. 3. The presence of the peaks assigned to the Ni–Ni and Ni–O bonds at 0.2 and 0.16 nm, respectively, indicated the formation of nano-sized Ni and NiO. The intensity of the Ni–Ni peak of the PAD-Ni-TiO_2-SiO_2 catalyst was less than that of the img-Ni-TiO_2-SiO_2 catalyst. This suggested that the size of the Ni metal particles depended on the preparation method and that smaller Ni particles were formed on the photo-deposited catalyst (PAD-Ni-TiO_2-SiO_2).

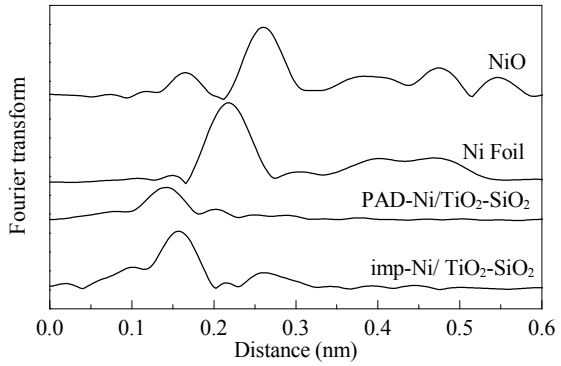

Fig. 3. Fourier transforms of Ni L_{III}-edge EXAFS spectra for PAD-Ni-TiO_2-SiO_2, img-Ni/TiO_2-SiO_2, Ni Foil, and NiO.

2.1.5 TEM observation

The TEM images of PAD-Ni-TiO_2-SiO_2 and img-Ni-TiO_2-SiO_2 catalysts are displayed in Fig. 4. The particle distributions obtained from the TEM images are displayed in Fig. 5. These data are in good agreement with the results obtained from XAFS measurement. Nano-sized Ni metal particles having a narrow size distribution (2–8 nm) were found on the PAD-Ni-TiO_2-SiO_2 catalyst, whereas aggregated Ni metal particles of larger sizes (10–25 nm) were observed on the img-Ni-TiO_2-SiO_2 catalyst. These data provide further evidence that the size of the Ni metal particles depended on the preparation method.

2.2 Evaluation of the catalytic activity

The photocatalytic activities of the samples were evaluated by photocatalytic H_2 production in an aqueous glucose solution under UV light irradiation. Figure 6 shows the amount of H_2 produced with illumination time in the photocatalytic reforming of glucose on the TiO_2-SiO_2 and Ni/TiO_2-SiO_2 catalysts. H_2 production on TiO_2-SiO_2 was negligible compared with that on the Ni/TiO_2-SiO_2 catalysts. The rate of H_2 production (slope of the lines in Fig. 6) was very much dependent on the preparation method and increased in the order, TiO_2-SiO_2 < imp-Ni/TiO_2-SiO_2 < PAD-Ni/TiO_2-SiO_2. This order is in agreement with the results obtained by the characterization tools: the smaller band

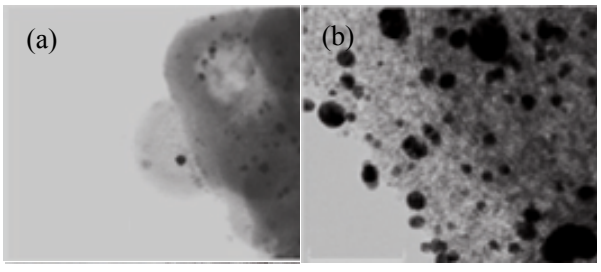

Fig. 4. TEM images of PAD-Ni-TiO_2-SiO_2 (a) and img-Ni-TiO_2-SiO_2 (b).

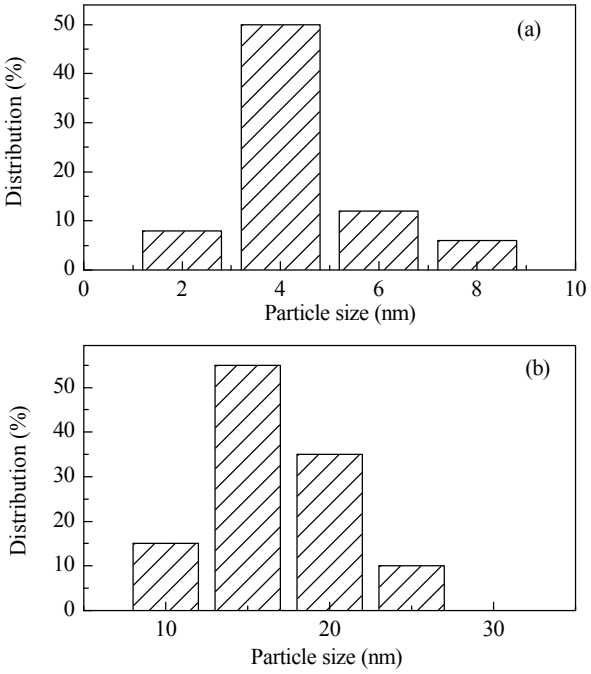

Fig. 5. Particle size distributions of Ni particles obtained from the TEM images of the PAD-Ni-TiO_2-SiO_2 (a) and img-Ni-TiO_2-SiO_2 (b) catalyst after treatment with H_2 at 473 K.

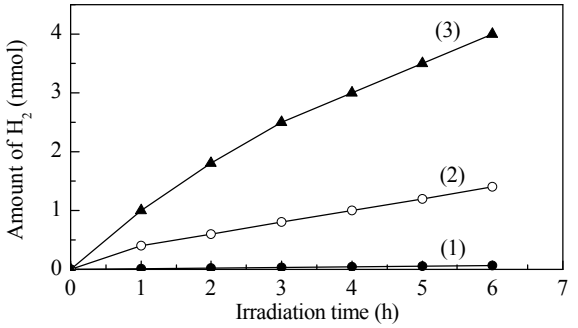

Fig. 6. Amount of H_2 produced in the photocatalytic reforming of glucose on TiO_2-SiO_2 (1), img-Ni-TiO_2-SiO_2 (2), and PAD-Ni-TiO_2-SiO_2 (3) as a function of irradiation time. Reaction conditions: 0.5 g catalyst, 1.25×10^{-3} mol/L glucose solution, 300 W Hg lamp light source, 300 ml glucose solution.

gap gave the higher photocatalytic activity (UV-Vis), the smaller particle size gave the higher surface area and photocatalytic activity (EXAF, TEM, and BET results).

From the consideration that pure Ni oxides do not possess photocatalytic oxidation properties, the variation in activity must be due to the same differences in the interaction between Ni and TiO_2-SiO_2 that led to the several changes in physical properties such as band gap, particle size, and surface texture. More importantly, we observed that the catalytic activity of TiO_2-SiO_2 increased with the addition of Ni. The maximum activity was obtained with PAD-Ni-TiO_2-SiO_2.

The correlation between the photoactivity and physical properties, such as band gap, surface area, and pore volume, is depicted in Fig. 7. Since the photocatalytic activity was highest in the case of PAD-Ni-TiO_2-SiO_2, this showed that maximizing the surface area and pore volume while minimizing the band gap provided the optimal result. It is believed that the lack of electron scavengers (surface Ti^{4+}) and hole traps (surface hydroxyl groups) were responsible for a rapid recombination rate of e^-/h^+, which leads to lower photocatalytic activity. The importance of decreasing the size of the band gap can be attributed to the lower energy needed to transfer an electron from the valance band to the conduction band. Therefore, PAD-Ni-TiO_2-SiO_2 exhibited the highest photoactivity because it has the smallest band gap and particle size and the highest surface area and pore volume.

Figure 8 shows the selectivity for CO (expressed as the molar ratio of CO/H_2). Much more CO was produced on TiO_2-SiO_2 than on the Ni/TiO_2-SiO_2 catalysts, indicating that CO production was greatly depressed on the supported Ni. CO selectivity, as was H_2 production, was largely de-

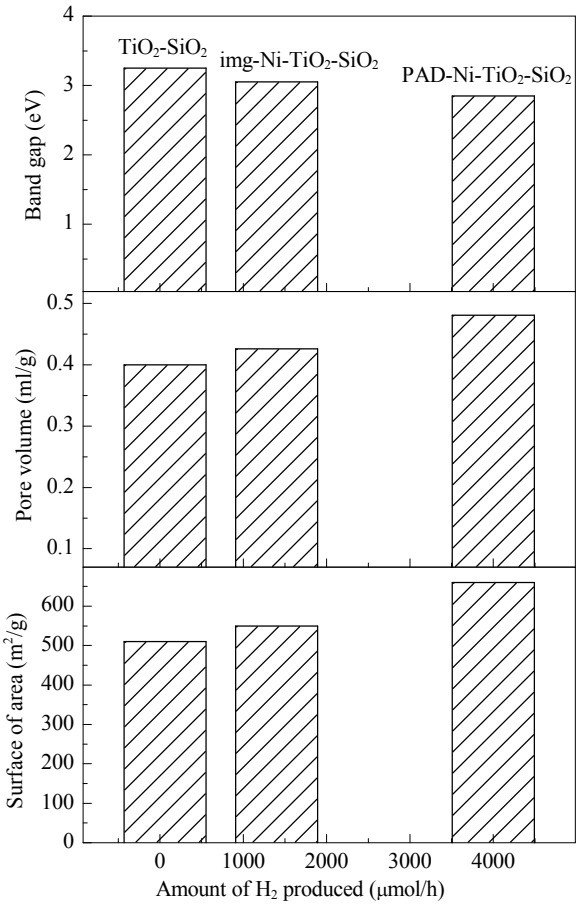

Fig. 7. Effect of the physical parameters of the materials on their photocatalytic activity.

pendent on the preparation method of the Ni/TiO_2-SiO_2 catalysts. The concentration of CO in H_2 was the lowest for the PAD-Ni/TiO_2-SiO_2 catalyst. Img-Ni/TiO_2-SiO_2 catalyst exhibited a much higher CO selectivity than PAD-Ni/TiO_2-SiO_2 catalyst, although the rate of H_2 production on Img-Ni/TiO_2-SiO_2 was relatively high. The fact that the photocatalytic activity was strongly dependent on the preparation method of the Ni/TiO_2-SiO_2 catalysts may be interpreted in terms of semiconductor theory. When Ni metal was deposited on TiO_2-SiO_2, the migration of excited electrons from the semiconductor TiO_2-SiO_2 to the Ni metal occurred until the two Fermi levels were aligned. The Schottky barrier formed at the Ni metal and TiO_2-SiO_2 interface can serve as an efficient electron trap that prevented photo-generated electron-hole recombination, which greatly enhanced the efficiency of the photocatalytic reaction. At the same time, the Ni metal is important because of its own catalytic activity. The Ni metal deposited on TiO_2-SiO_2 provided active sites for H_2 production, where trapped photogenerated electrons are transferred to protons to produce H_2 [52]. The CO selectivity of the Ni metal/TiO_2-SiO_2 catalyst can be explained by the mechanism of the photocatalytic reforming of glucose on TiO_2-SiO_2. John et al. [53] suggested that the hydroxyl and aldehyde functional groups in glucose underwent photocatalytic oxidation on a Pt/TiO_2 catalyst with the simultaneous production of carboxyls and protons. A formic acid species is formed in the reaction solution owing to the glucose molecule being continually oxidized and the C–C bond being broken. Therefore, it was assumed that the formic acid species is one of the intermediates in the glucose decomposition. It was suggested in a previous work that CO was produced via the decomposition of the intermediate formic acid species derived from methanol in the photocatalytic reforming of methanol [54,55]. When Ni metal was loaded on TiO_2-SiO_2, the catalyst promoted the HCOOH decomposition reaction to mainly H_2 and CO_2 products which suppressed the CO and H_2O products, resulting in much less CO being produced on Ni/TiO_2-SiO_2 than on TiO_2-SiO_2. On the other hand, the Ni actually modified the photocatalytic process of the semiconductor by changing the semiconductor surface properties [52]. The migration of excited electrons from the semiconductor TiO_2-SiO_2 to the Ni metal decreased the electron density of the semiconductor, leading to an increase in the hydroxyl group acidity [56]. This would affect the adsorption of glucose on TiO_2-SiO_2 surface. This in turn affects the photocatalytic process on the TiO_2-SiO_2 surface, which would result in enhancing or depressing a particular product, such as CO, or the rate of photocatalytic reaction. Different Fermi levels and other characteristic properties of the various metals lead to the CO selectivity being dependent on the kind of metal deposited on TiO_2.

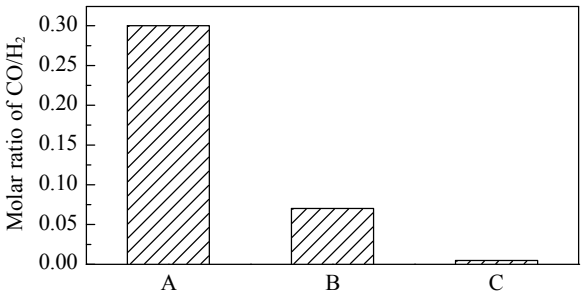

Fig. 8. The selectivity of CO (expressed as the molar ratio of CO/H_2) in the photocatalytic reforming of glucose on TiO_2-SiO_2 (A), img-Ni-TiO_2-SiO_2 (B), and PAD-Ni-TiO_2-SiO_2 (C). Reaction conditions: 0.5 g catalyst, 300 ml 1.25×10^{-3} mol/L glucose solution, 300 W Hg lamp, irradiation 1 h.

The mechanism of the photocatalytic reforming of glucose is described in Fig. 9. This includes (a) photogeneration of excited electrons, e^- and holes, h^+; (b) electron transfer to metal particles that reduce protons to form hydrogen molecules; (c) the holes continually oxidize H_2O, glucose, and its reaction products adsorbed on TiO_2-SiO_2, namely from H_2O and/or glucose to form various oxygen-containing species, CO, CO_2, and H^+.

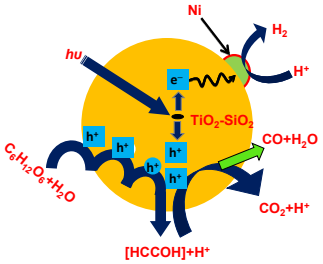

Fig. 9. Schematic of the photocatalytic reforming of glucose on Ni/TiO_2-SiO_2 catalysts.

3 Conclusions

Ni-TiO_2-SiO_2 catalysts were prepared by impregnation and photo-assisted deposition methods. The preparation method had a large effect on the size of the Ni metal particles. Both PAD- and img-Ni-TiO_2-SiO_2 were more active than the parent TiO_2-SiO_2 in photocatalytic oxidation and reduction. H_2 with a low CO concentration was produced by the photocatalytic reforming of glucose on TiO_2-SiO_2 and Ni/TiO_2-SiO_2 catalysts. The PAD-Ni/TiO_2-SiO_2 catalyst was very active for H_2 production with an ultra-low CO concentration due to its small band gap and large surface area, which was because the use of the PAD preparation method together with the TiO_2-SiO_2 material led to the deposition of nano-sized Ni metal particles on tetrahedrally coordinated titanium (IV) oxide with a well-controlled particle size and high dispersion. H_2 production from the photocatalytic

reforming of biomass on PAD-Ni/TiO_2-SiO_2 is promising for producing hydrogen for fuel cells.

Acknowledgements

This paper was funded by the Deanship of Scientific Research (DSR), King Abdulaziz University, Jeddah, under grant number (210-247/431). The authors, therefore, acknowledge with thanks DSR technical and financial support.

References

1 Goltsov V A, Veziroglu T N, Goltsov L F. *Int J Hydrogen Energy*, 2006, **31**: 153
2 Ni M, Leung D Y C, Leung M K H, Sumathy K. *Fuel Process Technol*, 2006, **87**: 461
3 Ni M, Leung M K H, Sumathy K, Leung D Y C. *Int J Hydrogen Energy*, 2006, **31**: 1401
4 Ni M, Leung M K H, Leung D Y C, Sumathy K. *Renewable Sustainable Energy Rev*, 2007, **11**: 401
5 Kato H, Kobayashi H, Kudo A. *J Phys Chem B*, 2002, **106**: 12441
6 Hara M, Hitoki G, Takata T, Kondo J N, Kobayashi H, Domen K. *Catal Today*, 2003, **78**: 555
7 Wu G, Chen T, Su W, Zhou G, Zong X, Lei Z, Li C. *Int J Hydrogen Energy*, 2008, **33**: 1243
8 Li Z H, Chen G, Liu J W. *Solid State Commun*, 2007, **143**: 295
9 Yuan Y, Zhang X, Liu L, Jiang X, Lv J, Li Z, Zou Z. *Int J Hydrogen Energy*, 2008, **33**: 5941
10 Liu J W, Chen G, Li H Z, Zhang G Z. *Int J Hydrogen Energy*, 2007, **32**: 2269
11 Zheng J X, Wei F L, Zhang H Z, Jiang J Q, Wei J Y, Xie B, Wei M. *Int J Hydrogen Energy*, 2009, **34**: 9033
12 Li C, Yuan J, Han B, Jiang L, Shangguan W. *Int J Hydrogen Energy*, 2010, **35**: 7073
13 Chen Y, Yang H, Liu X, Guo L. *Int J Hydrogen Energy*, 2010, **35**: 7029
14 Li Z, Chen G, Tian X, Li Y. *Mater Res Bull*, 2008, **43**: 1781
15 Li D, Chen J, Li Y. *Int J Hydrogen Energy*, 2009, **34**: 299
16 Li Y, Wang J, Peng S, Lu G, Li S. *Int J Hydrogen Energy*, 2010, **35**: 7116
17 Sreethawong T, Laehsalee S, Chavadej S. *Int J Hydrogen Energy*, 2008, **33**: 5947
18 Zou Z, Ye J, Sayama K, Arakawa H. *Nature*, 2001, **414**: 625
19 Wang L, Wang W, Shang M, Yin W, Sun S, Zhang L. *Int J Hydrogen Energy*, 2010, **35**: 19
20 Jing D, Liu M, Chen Q, Guo L. *Int J Hydrogen Energy*, 2010, **35**: 8521
21 Gautron J, Lemasson P, Poumellec B, Marucco J-F. *Sol Energy Mater*, 1983, **9**: 101
22 Fujishima A, Zhang X, Tryck D A. *Surf Sci Rep*, 2008, **63**: 515
23 Bouzoubaa A, Markovits A, Calatayud M, Minot C. *Surf Sci*, 2005, **583**: 107
24 Fujishima A, Hashimoto K, Watanabe T. TiO_2 Photocatalysis: Fundamentals and Applications. Tokyo: Bkc, 1999
25 Fujishima A, Zhang X. *C R Chimie*, 2006, **9**: 750
26 Bosc F, Ayral A, Keller N, Keller V. *Appl Catal B*, 2007, **69**: 133
27 Hidalgo C M, Maicu M, Navío A J, Colón G. *Catal Today*, 2007, **129**: 43
28 Linsebigler A L, Lu G Q, Yates J T. *Chem Rev*, 1995, **95**: 735
29 Fujishima A, Zhang X, Tryk D A. *Int J Hydrogen Energy*, 2007, **32**: 2664
30 Agrios A G, Pichat P. *J Photochem Photobiol A*, 2006, **180**: 130
31 Maurya S K, Patil P, Umbarkar S B, Gurjar M K, Dongare M, Rudiger S, Kemnitz E. *J of Mol Catal A*, 2005, **234**: 51
32 Bulushev D A, Rainone F, Kiwi-Minsker L. *Catal Today*, 2004, **96**: 195
33 Buscaa G, Liettib L, Ramisa G, Berti F. *Appl Catal B*, 1998, **18**: 1
34 Bellardita M, Addamo M, Di Paola A, Marcì G, Palmisano L, Cassar L, Borsa M. *J Hazard Mater*, 2010, **174**: 707
35 Sano T, Negishi N, Sakai E, Matsuzawa S. *J Mol Catal A*, 2006, **245**: 235
36 Kim J, Kim C, Chang H, Kim T. *Adv Powder Technol*, 2010, **21**: 141
37 Hamelinck C N, Faaij A P C. *J Power Sources*, 2002, **111**: 1
38 Bridgwater A V. *Appl Catal A*, 1994, **116**: 5
39 Huber G W, Shabaker J W, Dumesic J A. *Science*, 2003, **300**: 2075
40 Cortright R D, Davda R R, Dumesic J A. *Nature*, 2002, **418**: 964
41 Kawai T, Sakata T. *Chem Lett*, 1981: 81
42 Kawai T, Sakata T. *Nature*, 1980, **286**: 474
43 Yamashita H, Kawasaki S, Ichihashi Y, Harada M, Anpo M, Stewart G, Fox M A, Louis C, Che M. *J Phys Chem B*, 1998, **102**: 5870
44 Mohamed R M, Mkhalid I A. *J Alloys Compd*, 2010, **501**: 301
45 Mohamed R M, Mkhalid I A. *J Alloys Compd*, 2010, **501**: 143
46 Mohamed R M. *J Mater Processing Technol*, 2009, **209**: 577
47 Davis R J, Liu Z. *Chem Mater*, 1997, **9**: 2311
48 Kosuge K, Singh S. *Phys Chem B*, 1999, **103**: 3563
49 Belhekar A A, Awate S V, Anand R. *Catal Commun*, 2002, **3**: 453
50 Cheng S, Tsai J S, Lee F Y. *Catal Today*, 1995, **26**: 87
51 Zepeda T A, Martinez-Hernandez A, Guil-Lopez R, Pawele B. *Appl Catal B*, 2010, **100**: 450
52 Linsebigler A L, Lu G, Yates J T. *Chem Rev*, 1995, **95**: 735
53 John R M, Furgala A J, Sammells A F. *J Phys Chem*, 1983, **87**: 801
54 Wu G, Chen T, Zong X, Yan H, Ma G, Wang X, Xu Q, Wang D, Lei Z, Li C. *J Catal*, 2008, **253**: 225
55 Wu G, Chen T, Su W, Zhou G, Zong X, Lei Z, Li C. *Int J Hydrogen Energ*, 2008, **33**: 1243
56 Jafiezic-Renault N, Pichat P, Foissy A, Mercier R. *J Phys Chem*, 1986, **90**: 2733